AIMS Mathematics, 8(3): 7005–7020.
DOI: 10.3934/math.2023353
Received: 02 October 2022
Revised: 07 December 2022
Accepted: 15 December 2022
Published: 11 January 2023

http://www.aimspress.com/journal/Math

Research article

Numerical study of stagnation point flow of Casson-Carreau fluid over a continuous moving sheet

Muhammad Amin Sadiq Murad[1,*], Faraidun Kadir Hamasalh[2] and Hajar F. Ismael[3]

[1] Department of Mathematics, College of Science, University of Duhok, Duhok, Iraq
[2] Department of Mathematics, College of Education, University of Sulaimani, Sulaimani, Iraq
[3] Department of Mathematics, Faculty of Science, University of Zakho, Zakho, Iraq

* **Correspondence:** Email: muhammad.murad@uod.ac.

Abstract: This paper is devoted to analysis the behavior of heat transfer of Casson-Carreau fluid at the magnetohydrodynamic (MHD) stagnation point with thermal radiation over a continuous moving sheet. The suitable similarity transform is utilized to transfer the governing differential equations into a system of differential equations and then solve the converted non-linear system by the collocation technique based on the B-spline function (CTBS) and Runge-Kutta method (RK). The quasi-linearization technique is utilized to approach the non-linear equations of the model to a system of linear equations and used CTBS to acquire the solution of the system of linear equations. The obtained results are investigated with the present literature by direct comparison. It is found that an increment in the value of the Weissenberg number decreases the velocity profile and enhances the temperature profile for Casson and Carreau fluids. Conversely, increasing the values of the magnetic parameter, shrinking parameter, and Casson fluid parameter improve the velocity profile and depreciate the thermal distribution. Further, the temperature profile declines with an improvement in radiation parameter and Prandtl number for Casson and Carreau fluids. The influence of distinct physical parameters on the velocity and temperature profiles are depicted via tables and illustrative graphs.

Keywords: Casson-Carreau fluids; magnetohydrodynamic; collocation method; B-spline function; magnetic field
Mathematics Subject Classification: 65D07, 65M25, 76W05

1. Introduction

Magnetohydrodynamic stagnation point flow with thermal performance impact has implementations in various engineering processes such as blood flow models, polymer, and thinning and annealing of conductive material. Hiemenz [1] was the first to analyze the conventional 2D unsteady flow on a flat plate. Sakiadis [2] started an investigation on the flow through a continuous moving surface. Following that, several scholars continued to analysis the flow over an elongation sheet from a variety of perspectives [3–7]. However, the non-Newtonian flow is found in a various of large-scale industrial process such as blood flow models, polymer, thinning and annealing of conductive material, and ice flows. Furthermore, the Carrea fluid is one of a several non-Newtonian fluids. This type of non-Newtonian fluid is suitable to incompressible flows with higher and lower shear rates. Thus, it has advantages in numerous technological and production flows. Taking this into consideration, Georgiou [8] studied the time- dependent Micropolar fluid flows of a Carrea fluid with the existence of the slip impact and found that as the slip increases, the frequency and amplitude of oscillation in the radiate direction decrease. Naby et al. [9] studied heat transfer performance of Carreau fluid and focused on the peristalsis flow properties of Carreau fluid in the uniform canal. Magnetohydrodynamic is the physical characteristic that explains the behavior of a highly conducting fluid with the existent of an electric field. The conductive fluids produce an electrical current due to the liquid flow, and generated force increases the mechanistic behaviors of liquid. The electrically conducting peristaltic flow has considerable implementation in the biological fluids: such as blood flows, peristalsis flows, and nano fluid see [10–13]. The finite difference discretization (FDD) is used to study the radiation impact over magnetohydrodynamic boundary layer flow across heated shrinking surface [14]. Turkyilmazoglu in [15] studied the rotating flows in both stationary and rotational frames wall stretching in MHD. The Buongiorno nanofluid model is used to study the continuous 2D flow and heat transmission on a stretched surface of nanofluid [16]. A shear-thinning Cassion fluid is another kind of non-Newtonian fluid that generates the produce of shear stresses. Due to its rheological properties, it has been classified as the most widely used non-Newtonian fluid. The yield shear stress behaves like a solid when it is higher than the shear stress while the liquid begins to move when the yield shear stress is smaller than the shear stress, such as human blood, fruit juice, and tomato sauce. The Casson fluid has major applications in different aspects of real life like in cancer homeo-therapy and fibrinogen. Due to these significant advantages, it has been an area of interest to many researchers. A 3D Casson fluid through a thin linearly stretching surface with convection constrain is studied in [17]. 3D MHD stagnation point flow of incompressible Casson fluid in the porous material is studied via Shahzad [18]. 3D Casson-Carreau fluid in an unsteady stretched sheet is investigated by Raju and Sandeep [19]. The analysis of the Casson fluid flow on an expansion plate with the existent of the Dufour and Soret influences is studied in [20]. The dual solutions for a Casson fluid thermal properties and heat transfer enhancement on a porous continuous moving sheet are investigated in [21]. Aziz et al. [22] studied the magnetohydrodynamic Casson fluid across stretched surface for viscous dissipation estimation and Hall impacts. Very recently, heat transfer and stagnation-point flow over elastic sheets and cylinders with an incoming flow is analyzed by Mustafa [23]. Ali et al. investigated the thermal variations for Cattaneo-Christov characteristics and self-induced bioconvective microorganisms submerged in the water nanofluid and the boundary layer flow across a wedge with an unstable MHD stagnation point see [24–27]. Further, Mahabaleshwar et al. in [28] studied the THD attribution of boundary layer incompressible viscous

fluid with two types of carbon nanotubes (CNTs). Finally, the influence of morphological nanolayer on the MHD nanofluid flow is studied in [29]. The magnetohydrodynamic micropolar ferrofluid flow and heat transfer over stretching sheet is analyzed in [30].

The main object of the present paper is to extend the study of magnetohydrodynamic stagnation points flow of Casson-Carreau fluid electrically conducting in the existent of thermal radiation and transverse magnetic field. The proposed model has significance in different industrial as well as technological applications and applied sciences. The Maple 2020 program is employed to solve the converted mathematical problem using the Runge Kutta method (RK) and the collocation method based on the B-spline function. The present results are compared with that those reported in [14,31,32]. The numerical and graphical representations of the influence of emerging parameters on velocity and thermal distributions are provided.

2. Mathematical model

Consider 2D magnetohydrodynamic stagnation point flow of an incompressible viscous Casson-Carreau fluid flow electrically conducting intruding regularly over heated continuous moving plate. Assume that the magnetic Renolds parameter is represented by small Shercliff [33] and the velocity field and the uniform stationary magnetic field of strength B are perpendicular. Here, the produced magnetic field is disregarded compare to the force field. The electric field is zero, no polarization voltage is supplied with the valid the boundary layer and the Boussinesq approximations see Figure 1. The equations of motion of steady 2D magnetohydrodynamic incompressible viscous Casson-Carreau fluid flow is given as follows:

$$\begin{aligned} &z_x + w_y = 0, \\ &zz_x + wz_y = \frac{-p_x}{\rho} + \frac{\lambda}{\rho} z_{ww} + \nu\left(1+\frac{1}{\beta}\right) z_{ww} + \frac{\sigma_e B_0{}^2}{\rho}(Z-z) + \nu\left(\frac{3n-3}{2}\right)\Gamma^2 z_{yy} z_y^2. \end{aligned} \tag{2.1}$$

The electric conductivity of the fluid is σ, pressure represented p and Z represents the free stream velocity.

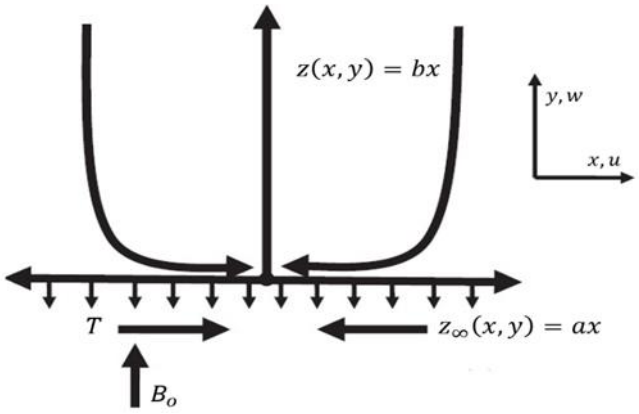

Figure 1. The sketch of the present model.

In the absence of the viscous dissipation the thermal allocation equation for our boundary value problem is as follows [14]:

$$\rho c\left(zT_x + wT_y\right) = \kappa_0 T_{yy} - q_y, \tag{2.2}$$

when is the given thermal ability at fixed pressure, represents the temperature, represents the heat conductivity constant, and is the radiative thermal flux. The radiative thermal flow using Resseland approximation [34] is simplified as follows:

$$q = \frac{4\sigma}{3k} T_y^4, \tag{2.3}$$

when σ represents the mean absorption parameter and k represents the Stefan-Boltzmann number.

T^4 represents the thermal fluctuation inside the flow which is considered to be a linear function of temperature. Appling the Taylor series about T^∞ for expanding T^4

$$T^4 \simeq T_\infty^3 (4T - 3T_\infty). \tag{2.4}$$

Taking Eq (2.3) and Eq (2.4), the Eq (2.2) is reduced to

$$zT_x + wT_y = \frac{1}{\rho c}\left(k_0 + \frac{16\sigma T^3{}_\infty}{3k}\right) T_{yy}. \tag{2.5}$$

The above equation depicts that the enhance of thermal conductivity is due to the impact of radiation. Assume that $Nr = \frac{kk_0}{4\sigma T^3{}_\infty}$ is the radiation parameter. Thus, Eq (2.5) becomes

$$zT_x + wT_y = \frac{k_0}{k} T_{yy}, \tag{2.6}$$

where $k = \frac{Nr}{Nr + \frac{4}{3}}$.

Consider the following boundary conditions regarding the proposed problem

$$\begin{aligned} &z(x,y) = bx, w(x,y) = 0, \; T(x,y) = T_0, y \to 0 \\ &z_\infty(x,y) = Z_\infty = ax, \qquad T(x,y) = T_\infty, y \to \infty. \end{aligned} \tag{2.7}$$

Here, $z_\infty(x,y)$ and $z(x,y)$ represent the velocities close to and far from the wall, respectively. $b > 0$ represents the shrinking ratio, T_0 represents the thermal sheet, T_∞ is a representation of the fluid temperature beyond the boundary layer, and $(T_0 > T_\infty)$. Now, solving governing Eqs (2.1) and (2.6) with the given boundary conditions (2.7) gives the velocity and thermal fields for the proposed model. Hence, the following similarity transform is given

$$\eta = \left(\frac{a}{\nu}\right)^{0.5} y,\ p(x,\infty) = p_0 - \frac{1}{2}\left(x^2 + y^2\right)a^2\rho,$$
$$z(x,y) = xaf'(\eta),\ w(x,y) = -f(\eta)\left(a\nu\right)^{0.5}, \tag{2.8}$$
$$\theta(\eta) = \left(T - T_\infty\right)\left(T_0 - T_\infty\right)^{-1},$$

when η represents the similarity parameter, p_0 and a are the strength of stagnation point and the stagnation pressure respectively. Satisfying the Eq (2.8) in Eq (2.1), the continuity Eq (2.1) satisfied and the possible fluid motion is represented by velocity field, and then putting Eq (2.8) in Eq (2.1) with some simple calculations, we obtain

$$\left(1+\frac{1}{\beta}\right)f''' + \frac{3}{2}(n-1)We\, ff'''f''^2 + ff'' - f''^2 - M^2\left(f'-1\right)+1 = 0. \tag{2.9}$$

Putting Eq (2.8) in Eq (2.6), we obtain

$$\frac{1}{\Pr}\theta'' + k\,\theta' f = 0. \tag{2.10}$$

Now, $M = \left(\frac{B_0^2\sigma_e}{a\rho}\right)^{0.5}$ is magnetic field parameter or (Hartmann number) and $\Pr = \frac{c\mu}{\kappa_0}$ Prandtl number. Also, $k = \frac{3Nr}{3Nr+4}$ where Nr represents the radiation parameter.

The considered conditions in (2.7) with taking the dimensionless parameters in consideration, we obtain

$$f(0) = 0,\ f'(0) = B = \frac{b}{a},\ \ f'(\infty) = 1,$$
$$\theta(0) = 1, \theta(\infty) = 0. \tag{2.11}$$

Here, the novelty of the present model is that the magnetohydrodynamic stagnation points flow of a new model of Casson-Carreau fluid on a continuous moving surface electrically conducting in the existing of thermal radiation and transverse magnetic field has been studied.

3. Quartic B-spline method

In this portion, we devote to determine a brief description of B-spline function. Here, the domain $[\tilde{a},\tilde{b}]$ is split into N distinct partition and the set of knots $S = \left\{\tilde{a}, s_1, s_2, ..., s_{N-1}, \tilde{b}\right\}$ is named by knot vector. The B-spline is introduced depends on $S = \left\{\tilde{a}, s_1, s_2, ..., s_{N-1}, \tilde{b}\right\}$. The recursion formula of the high degree B-splines is defined as follows:

$$B_j^l(x) = \frac{x - s_j}{s_{j+l} - s_j} B_j^{l-1}(x) + \frac{s_{j+l+1} - x}{s_{j+l+1} - s_{j+1}} B_{j+1}^{l-1}(x),\ \ j = 1,2,3,... \text{ and } \ l = 1,2,3,....$$

The zero-degree B-splines are introduced by:

$$B_j^0(x) = \begin{cases} 1 & s_j \le x \le s_{i+1} \\ 0 & otherwise. \end{cases}$$

The explicit less common formula is defined by:

$$B_j^l(x) = \frac{1}{l!}\sum_{m=0}^{l+1}\binom{l}{m}(-1)^m\left(x+\frac{l+1}{2}-m\right)_+^l .$$

Assume that the knot vector contains a set of integers defined on the domain. Thus, the uniform B-spline functions are obtained from the B-spline formula. The integration and derivation forms are as follows [35,36].

$$\frac{d}{dx}B_j^l(x) = \frac{l}{s_{j+l}-s_j}B_j^{l-1}(x) - \frac{l}{s_{j+l+1}-s_{j+1}}B_{j+1}^{l-1}(x), \quad \int_{-\infty}^{x} B_j^l(t)dt = \frac{s_{j+l+1}-s_{j+1}}{l+1}\sum_{i=j}^{\infty}B_i^{l+1}(x) .$$

To obtain the high accuracy approximate solution of the present model utilizing B-spline of degree l, it needs to provide $s_{-l}, s_{-l+1}, ..., s_{-1}$ and $s_{N+1}, s_{N+2}, ..., s_{N+k}$ to the determined collection s. Thus, the generated functions span the model interval evenly. Let $B = \{B_{-l}, B_{-l+1}, ..., B_N\}$ represents the basis function set for $[\tilde{a}, \tilde{b}]$.

Suppose $H(x)$ is the numerical solution of the present model which has the following form

$$H(x) = \sum_{j=-l}^{N} c_j B_j(x) . \tag{3.1}$$

In the present study, we propose to compute at Gaussian points of the chosen domain instead of normal points to obtain the faster convergence of the collocation technique [37]. It is worth noting that the colocation points that appear at the zeros of determined basis functions give promising results [38].

4. Quasi linearization technique (QLT)

To approach a non-linear ordinary differential equation (ODE) to a linear ODE the QLT algorithm is used. The technique depends on Newton-Raphson technique which was found by Mandelzweig and Tabakin [39]. The QLT is widely utilized in different fields of science like applied mathematics and astronomy [40]. The approximate linear ODE driven by QLT cannot be solved analytically, thus the collocation technique based on B-spline function is proposed to study the proposed problem numerically. Here, we apply the QLT to the present problem the approximate linear differential equation at the $(m+1)$ iteration given by:

$$\begin{aligned}\frac{d^3 f}{d\eta^3} &= \Omega(f''(\eta), f'(\eta), f(\eta), \eta),\\ \frac{d^2\theta}{d\eta^2} &= \Theta(\theta'(\eta), \theta(\eta), \eta).\end{aligned} \tag{4.1}$$

Using Eq (2.9) and Eq (2.10), we get

$$\Omega\left(\eta, f(\eta), f'(\eta), f''(\eta)\right) = \frac{f'(\eta) f'(\eta) - f(\eta) f''(\eta) - \left(1 - f'(\eta)\right) M^2 - 1}{\left(1 + \frac{1}{\beta}\right) + \frac{3}{2}(n-1)\, f''(\eta)^2 We},$$

$$\Theta\left(\eta, \theta(\eta), \theta'(\eta)\right) = -\Pr k\, \theta'(\eta) f(\eta).$$

The QLT formula is given as follows:

$$\begin{aligned}&\frac{d^3 f_{m+1}}{d\eta^3} = \Omega(f_m'', f_m', f_m, \eta) - \Omega_f(f_m'', f_m', f_m, \eta)(f_m - f_{m+1}) - \Omega_{f'}(f_m'', f_m', f_m, \eta)(f_m' - f_{m+1}')\\ &-\Omega_{f''}(f_m'', f_m', f_m, \eta)(f_m'' - f_{m+1}''),\\ &\frac{d^2\theta}{d\eta^2} = \Theta(\theta_m', \theta_m, \eta) - \Theta_\theta(\theta_m', \theta_m, \eta)(\theta_m - \theta_{m+1}) - \Theta_{\theta'}(\theta_m', \theta_m, \eta)(\theta_m' - \theta_{m+1}').\end{aligned} \tag{4.2}$$

Associate with the boundary conditions:

$$\begin{aligned}&f_{m+1}(0) = 0,\ f_{m+1}'(0) = B,\ f_{m+1}'(\infty) = 1,\\ &\theta_{m+1}(0) = 1, \theta_{m+1}(\infty) = 0,\end{aligned} \tag{4.3}$$

when m is the iteration number.

The above conditions at zero are satisfied by the initial guesses $f_0(\eta) = B\eta$ and $\theta_0(\eta) = 1$. The solution of the proposed model is studied numerically utilizing the B-spline basis:

$$f_m(\eta) = \sum_{j=-l}^{N} c_{j,m} B_j(\eta) \text{ and } \theta_m(\eta) = \sum_{j=-l}^{N} a_{j,m} B_j(\eta)\,. \tag{4.4}$$

Here, we choose the following assignments instead of the initial guesses satisfy the boundary conditions at zero:

$$\tilde{f}_m(\eta) = B\eta + \eta^2 f_m \text{ and } \theta_m(\eta) = 1 + \eta\theta_m\,. \tag{4.5}$$

Now, $\tilde{f}_m$ and θ_m satisfy the first and second conditions of the stream function and first condition of the heat function, respectively.

The following residual equations at each iteration are obtained after substituting $\tilde{f}_m$ and θ_m from system (4.2) into (4.1)

$$\mathrm{Re}s_m^f(\eta)=\tilde{f}_{m+1}'''+\frac{\tilde{f}_m'^2-\tilde{f}_m\tilde{f}_m''-M^2(1-\tilde{f}_m')-1}{\left(\frac{3}{2}(n-1)We\,\tilde{f}''^2+\left(1+\frac{1}{\beta}\right)\right)}+\left(\tilde{f}_m-\tilde{f}_{m+1}\right)\frac{-\tilde{f}_m''}{\left(\frac{3}{2}(n-1)We\,\tilde{f}_m''^2+\left(1+\frac{1}{\beta}\right)\right)}$$

$$+\left(\tilde{f}_m'-\tilde{f}_{m+1}'\right)\frac{2\tilde{f}_m'+M^2}{\left(\frac{3}{2}(n-1)We\,\tilde{f}_m''^2+\left(1+\frac{1}{\beta}\right)\right)},$$

$$+\left(\tilde{f}_m''-\tilde{f}_{m+1}''\right)\frac{-\tilde{f}_m\left(\frac{3}{2}(n-1)We\,\tilde{f}_m''^2+\left(1+\frac{1}{\beta}\right)\right)-\left(\tilde{f}_m'^2-\tilde{f}_m\tilde{f}_m''-M^2(1-\tilde{f}_m')-1\right)\left(3(n-1)We\,\tilde{f}_m''\right)}{\left(\frac{3}{2}(n-1)We\,\tilde{f}_m''^2+\left(1+\frac{1}{\beta}\right)\right)^2}.$$

$$\mathrm{Re}s_m^\theta(\eta)=\tilde{\theta}_{m+1}''-\tilde{\theta}_{m+1}'\,\mathrm{Pr}\,k\,\tilde{f}_m.$$

Here, we have constructed a system of $2N+2k-1$ equations, our goal is to reduce the residuals by collocating at each point. Using LU-factorization methodology to find the value of coefficients $c_{j,m}$ and $a_{j,m}$ which are utilized to form $\tilde{f}_m$ and $\tilde{\theta}_m$ as a supposition for the next iteration's solution.

$$B_i(s)=\begin{cases}(s-s_{i-2})^4, & s_{i-2}\le s\le s_{i-1},\\ h^4+4h^3(s-s_{i-1})+6h^2(s-s_{i-1})^2+4h(s-s_{i-1})^3-4(s-s_{i-1})^4, & s_{i-1}\le s\le s_i,\\ 11h^4+12h^3(s-s_i)-6h^2(s-s_i)^2-12h(s-s_i)^3+6(s-s_i)^4, & s_i\le s\le s_{i+1},\\ h^4+4h^3(s_{i+2}-s)+6h^2(s_{i+2}-s)^2+4h(s_{i+2}-s)^3-4(s_{i+2}-s)^4, & s_{i+1}\le s\le s_{i+2},\\ (s_{i+3}-s)^4, & s_{i+2}\le s\le s_{i+3},\\ 0, & \textit{otherwise.}\end{cases} \tag{4.6}$$

The function $B_i(s)$ is locally supported non-negative over $[s_{i-2},s_{i+3}]$.

Table 1 is used to find and its derivatives.

Table 1. Coefficient of quartic B-splines and its derivatives at nodes s_j.

S	s_{j-2}	s_{j-1}	s_j	s_{j+1}	s_{j+2}	s_{j+3}
$B_j(z)$	0	$\frac{1}{24}$	$\frac{11}{24}$	$\frac{11}{24}$	$\frac{1}{24}$	0
$hB_j'(z)$	0	$\frac{1}{6}$	$\frac{1}{2}$	$\frac{-1}{2}$	$\frac{-1}{6}$	0
$h^2B_j''(z)$	0	$\frac{1}{2}$	$\frac{-1}{2}$	$\frac{-1}{2}$	$\frac{1}{2}$	0
$h^3B_j'''(z)$	0	1	-1	1	-1	0

5. Results and discussion

In this portion, the gained approximate solutions using collocation technique based on B-spline function (4.4) are discussed. The condition $f'(G)=1$ is used instead of the condition $f'(\infty)=1$ for some sufficiently large G [41]. The solution obtained by CTBS of the proposed problem is investigated to show the characteristic of Casson and Carreau fluid flow for various magnetic field and velocity parameter values. The non-dimensional parameters are considered as $\mathrm{Pr}=0.7$, $M=1,n=2,We=1,B=-0.5,\beta=\infty$ and $Nr=3$ in numerical results except the variations. In

illustrative graphs, the red color profiles and blue color profiles are signalize the flow of Casson fluid and the flow of Carreau fluid, respectively. Figure 2 describes the impact of B on the velocity distribution for Casson and Carreau fluids. The natural velocity $f(\eta)$ and the horizontal velocity $f'(\eta)$ improve with increasing magnitude of shrinking parameter B. Hence, as the value of B decreases the velocity becomes thicker. Here, we deduce that for high values of the shrinking parameter, the stretches of the vertical flow regime grow as the horizontal flow reversal induces the vertical flow reversal in the region around the stagnation point. Figure 3 demonstrates the strength of the magnetitic field parameter on the solutions $f(\eta)$ and velocity distribution. We find that the normal $f(\eta)$ and the horizontal velocities profiles $f'(\eta)$ are enhanced with increment of values M. The impact of the values of shrinking and magnetic parameters on the thermal profiles is shown in Figure 4 for Casson and Carreau fluids.

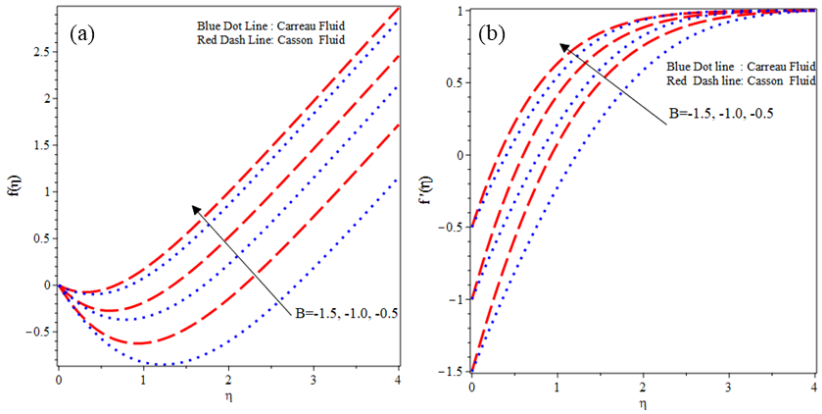

Figure 2. The solution of CTBS $f(\eta)$ and $f'(\eta)$ for several values of B.

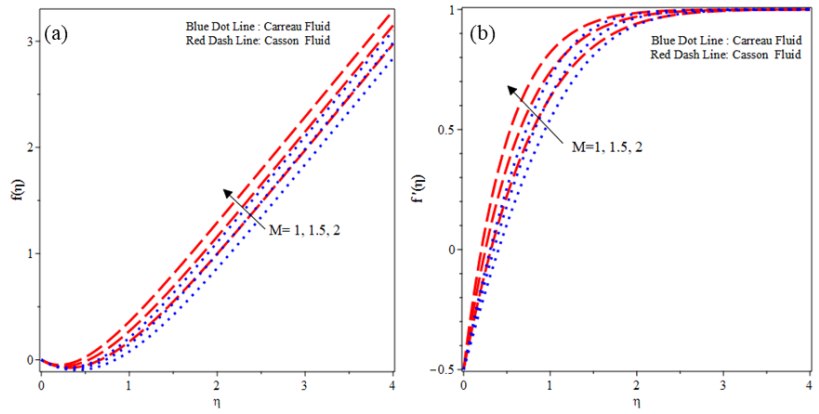

Figure 3. The solution of CTBS $f(\eta)$ and $f'(\eta)$ for several values of M.

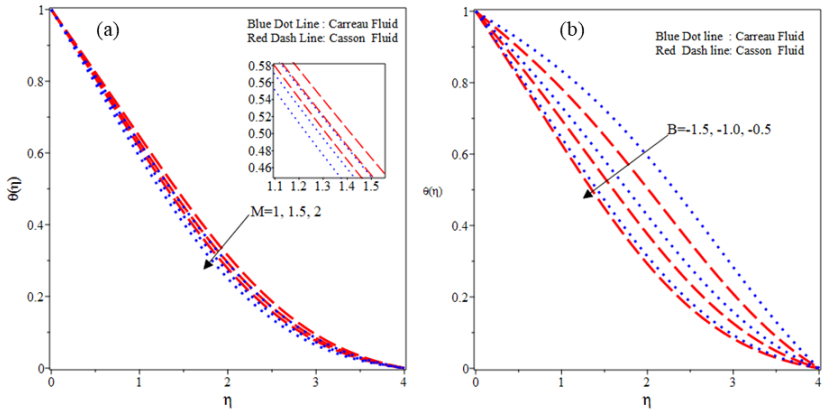

Figure 4. Influence of M and velocity parameter B on temperature profiles.

In Figure 4 increasing the values of B cases depreciation in the temperature profiles. Further, the magnetic field supports the impinging flux which decreases the amplitude of both reversal regime flows and makes the thermal boundary layer thickness and hydrodynamic to decline and become thinner. The impact of the Weissenberg number We on the solutions and velocity distributions is displayed in Figure 5 for both Casson and Carreau fluids. From Figure 5 we observe that the solutions and the velocity distributions enhance with decreasing in the value of the Weissenberg number. From Figure 7 on can observe that the thermal distributions experience a growth trend via increasing the value of Weissenberg number. Physically, the Weissenberg number is reversely proportional to the viscosity yet linearly proportional to the time constant. For bigger ratios of Weissenberg number, the time constant to viscosity ratio is higher. Hence, the improvement in the values of We increase the thermal boundary thickness. Figure 6 describes the effect of the dimensionless Casson fluid coefficient on the solution and velocity profiles of both fluids. It reveals that a hike in the value of improves the solutions and velocity profiles. In contrast, we observed depreciation in the thermal distributions in Figure 7 due to increasing the values of dimensionless Casson fluid number. Finally, in Figure 8 the impact of Prandtl number $\Pr$ and radiation parameter Nr on the thermal distributions are elucidated for both fluids. From Figure 8 one can observe that the thermal boundary thickness is declined with increment in the value of $\Pr$. The same behavior can be observed with improving values of Nr. Hence, for larger Prandtl number the liquid has a low temperature conductivity, that decline the correspondent thermal boundary thickness. Thus, the rate of heat transfer is increased at the plate with rising Prandtl number. Further, for higher radiation parameter the thinning of the thermal boundary thickness is occurred. Here, one can utilize the radiative mode of thermal transmission to enhance the sheet heat loss. This is normal because there are now two different ways of heat transfer proportion that govern the temperature resistance at the heat transfer sheet.

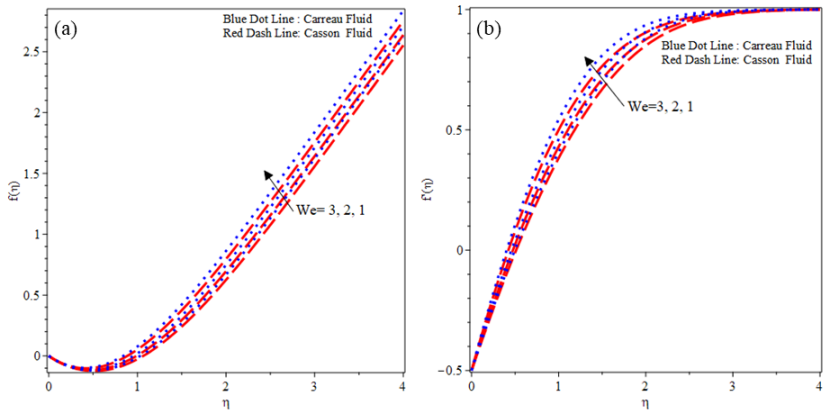

Figure 5. The solution of CTBS $f(\eta)$ and $f'(\eta)$ for several values of We.

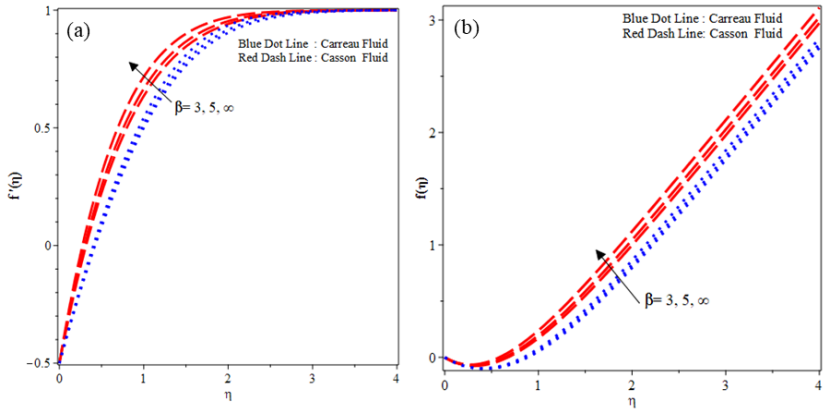

Figure 6. The solution of CMBS $f(\eta)$ and $f'(\eta)$ for several values of β.

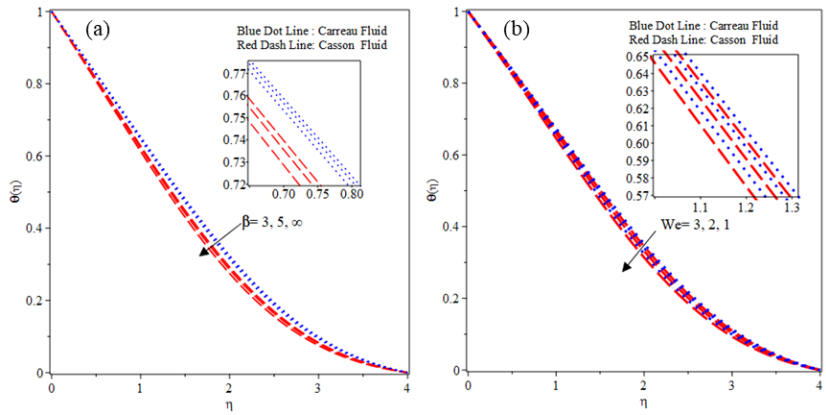

Figure 7. Influence of β and We on temperature profiles.

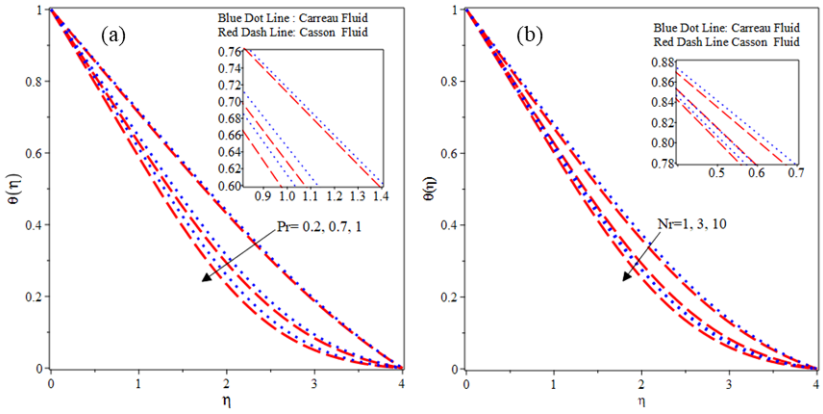

Figure 8. Effect of Pr and Nr on temperature profiles.

Table 2 illustrates the comparison of values of $f''(0)$ and $-\theta(0)$ at the sheet for several values of velocity parameter with the existent of magnetic field. The skin friction rises for $0.25 \le -B \le 1.25$. Conversely, an adverse trend has been observed for $1.25 \le -B \le 2.0$. The non-monotonic properties of skin friction versus the shrinking parameter are also been shown via Wang [32]. Physically, as shown in Figure 2 The vertical propagation proportion of the level flow reflection region and hence boundary of the layer is not steady with improvement in the value of shrinking parameter. However, $-\theta(0)$ rises due to incrementing values of shrinking parameter. The same behavior can be observed in Table 3 with the presence of Casson fluid parameter and Carreau fluid parameter. Table 4 demonstrates the impact of implement magnetic field M on $f''(0)$ and $-\theta(0)$. Clearly, the values of shear stresses increase due to improvement in the values of M while the rate of the heat transfer from the surface experience a decline with an enhancement in the values of M. Hence, the impinging flow is assisted by the transverse magnetic field and decreases the horizontal and vertical flow reversal as depicted in Figure 3. The same behavior is observed in Table 5 with the presence of Casson fluid parameter and Carreau fluid parameter. Finally, in Table 6 the comparison of values of skin friction and heat transfer rate is given. We deduced from tables that the acquired results employing proposed technique are in an excellent agreement with that of Wang [32], Lok [31], Ashraf and Rashid [14], and Runge-Kutta method.

Table 2. The effect of B on $f''(0)$ and $-\theta'(0)$.

$-B$	CTBS $f''(0)$	CTBS $-\theta'(0)$	FDD [14] $f''(0)$	FDD [14] $-\theta'(0)$	RK $f''(0)$	RK $-\theta'(0)$
0.25	1.877458	0.411450	1.877455	0.412803	1.877460	0.411444
0.50	2.120148	0.377394	2.120114	0.378822	2.120190	0.377390
1.00	2.429951	0.300877	2.429972	0.302334	2.429962	0.300867
1.25	2.476297	0.256815	2.476343	0.258227	2.476281	0.256804
1.50	2.425857	0.207058	2.425917	0.208447	2.425803	0.207043
2.00	1.805775	0.076266	1.805761	0.076282	1.805569	0.076248

Table 3. The effect of B on $f''(0)$ and $-\theta'(0)$.

B	Carreau fluid $f''(0)$	Carreau fluid $-\theta'(0)$	Casson fluid $f''(0)$	Casson fluid $-\theta'(0)$
-0.5	1.366443	0.340120	1.836118	0.360010
-1.0	1.479759	0.236458	2.10440	0.276883
-1.5	1.463260	0.123325	2.100834	0.177310
-2.0	1.181024	0.021825	1.563769	0.051355

Table 4. The effect of M on $f''(0)$ and $-\theta'(0)$.

M	CTBS $f''(0)$	CTBS $-\theta'(0)$	RK $f''(0)$	RK $-\theta'(0)$	FDD [14] $f''(0)$	FDD [14] $-\theta'(0)$
0.0	1.495673	0.346041	1.495673	0.346037	1.495722	0.346172
0.5	1.674182	0.356415	1.674189	0.356411	1.674222	0.356736
1.0	2.120147	0.378352	2.120190	0.378348	2.120137	0.379832
1.5	2.703645	0.400742	2.703762	0.400735	2.703497	0.405899

Table 5. The effect of magnetic field parameter M on $f''(0)$ and $-\theta'(0)$.

M	Carreau fluid $f''(0)$	Carreau fluid $-\theta'(0)$	Casson fluid $f''(0)$	Casson fluid $-\theta'(0)$
0.0	1.086783	0.314312	1.2952935	0.327178
0.5	1.172461	0.322615	1.449889	0.338060
1.0	1.366443	0.340120	1.836118	0.360010
1.5	1.588259	0.358007	2.341526	0.384884

Table 6. Comparison of values of $f''(0)$ for stretching parameter B.

B	CTBS	FDD[14]	RK	Wang[32]	Lok[31]
0.2	1.05113	1.05112	1.05113	1.05113	1.05129
0.5	0.71330	0.71328	0.71329	0.71330	0.71334

6. Conclusions

This work considers the 2D MHD stagnation point Casson-Carreau fluid flow on a continuous moving surface and thermal convey of an electrically conducting fluid towards a heated shrinking sheet. The quasi-linearization method utilized to transfer the non-linear equations of the problem to a system of linear equations and then solve the obtained nonlinear system via the developed collocation technique based on the B-spline function. The comparison of the acquired results with the solutions already found illustrates the efficiency of the suggested technique. Further, we discussed the influence of crucial physical parameters like magnetic field number, shrinking parameter, Casson fluid parameter, Prandtl number, radiation parameter, and Weissenberg number on the velocity and thermal distributions for both Casson and Carreau fluids. This work has shown that:

(i). The thermal profiles depreciate with improvement in the values of Prandtl number and radiation parameter for both fluids. Thus, the temperature distribution is decreased when the

temperature radiation term is present in the energy equation.

(ii). The temperature profiles experience a decline with increasing in the value of each of dimensionless Casson fluid parameter, shrinking parameter, and magnetic field parameter, while the thermal profile faces an increment with enhancement in the value of for Casson fluid and Carreau fluid.

(iii). Increasing the value of the Weissenberg number causes depreciation in the velocity profile for both Casson and Carreau fluids while an increment in the values of the other physical parameters enhance the velocity distributions.

(iv). The shear stress significantly affected by the value of the shrinking parameter. The value of the shear stress improves for $0.25 \leq -B \leq 1.25$. Conversely, an adverse trend can be observed for $1.25 \leq -B \leq 2.0$. Meanwhile, for both cases the rate of the heat transfer experiences an improvement due to increment in the values of B.

(v). The magnetic field also effects on the skin friction and the rate of the heat transfer. The skin friction enhances due to increment in the magnetic field parameter for both fluids while the rate of the heat transfer depreciates when the value of magnetic parameter improves. In future, one can utilize the developed collocation method based on B-spline functions to study the solutions of boundary layer problems.

Conflict of interest

The authors declare no conflict of interest.

References

1. K. Hiemenz, Die Grenzschicht an einem in den gleichformigen Flussigkeitsstrom eingetauchten geraden Kreiszylinder, *Dinglers Polytech. J.*, **326** (1911), 321–324.
2. B. Sakiadis, Boundary-layer behavior on continuous solid surfaces: II, the boundary layer on a continuous flat surface, *AiChE J.*, **7** (1961), 221–225. https://doi.org/10.1002/aic.690070211
3. B. Sakiadis, Boundary-layer behavior on continuous solid surfaces: III. the boundary layer on a continuous cylindrical surface, *AiChE J.*, **7** (1961), 467–472. https://doi.org/10.1002/aic.690070325
4. L. Crane, Flow past a stretching plate, *Z. Angew Math. Phys.*, **21** (1970), 645–647. https://doi.org/10.1007/BF01587695
5. P. Gupta, A. Gupta, Heat and mass transfer on a stretching sheet with suction or blowing, *Can. J. Chem. Eng.*, **55** (1977), 744–746. https://doi.org/10.1002/cjce.5450550619
6. P. Carragher, L. Crane, Heat transfer on a continuous stretching sheet, **62** (1982), 564–565. https://doi.org/10.1002/zamm.19820621009
7. D. Malo, R. Masiha, M. Murad, S. Abdulazeez, A new computational method based on integral transform for solving linear and nonlinear fractional systems, *Jurnal Matematika MANTIK*, **7** (2021), 9–19. https://doi.org/10.15642/mantik.2021.7.1.9-19
8. G. Georgiou, The time-dependent, compressible Poiseuille and extrudate-swell flows of a Carreau fluid with slip at the wall, *J. Non-newton Fluid*, **109** (2003), 93–114. https://doi.org/10.1016/S0377-0257(02)00164-7
9. A. El Hakeem, A. El Misery, M. El Kareem, Separation in the flow through peristaltic motion of a Carreau fluid in uniform tube, *Physica A*, **343** (2004), 1–14. https://doi.org/10.1016/j.physa.2004.05.072

10. M. Murad, Modified integral equation combined with the decomposition method for time fractional differential equations with variable coefficients, *Appl. Math. J. Chin. Univ.*, **37** (2022), 404–414. https://doi.org/10.1007/s11766-022-4159-5
11. T. Hayat, N. Saleem, N. Ali, Effect of induced magnetic field on peristaltic transport of a Carreau fluid, *Commun. Nonlinear Sci.*, **15** (2010), 2407–2423. https://doi.org/10.1016/j.cnsns.2009.09.032
12. N. Sandeep, V. Sugunamma, P. Mohan Krishna, Effects of radiation on an unsteady natural convective flow of a EG-Nimonic 80a nanofluid past an infinite vertical plate, *Advances in Physics Theories and Applications*, **23** (2013), 36–43.
13. M. Murad, Property claim services by compound Poisson process and inhomogeneous Levy process, *Science Journal of University of Zakho*, **6** (2018), 32–34. https://doi.org/10.25271/2018.6.1.420
14. M. Ashraf, M. Rashid, MHD boundary layer stagnation point flow and heat transfer of a micropolar fluid towards a heated shrinking sheet with radiation and heat generation, *World Appl. Sci. J.*, **16** (2012), 1338–1351.
15. M. Turkyilmazoglu, Wall stretching in magnetohydrodynamics rotating flows in inertial and rotating frames, *J. Thermophys. Heat Tr.*, **25** (2011), 606–613. https://doi.org/10.2514/1.T3750
16. K. Zaimi, A. Ishak, I. Pop, Flow past a permeable stretching/shrinking sheet in a nanofluid using two-phase model, *PLoS One*, **9** (2014), 111743. https://doi.org/10.1371/journal.pone.0111743
17. G. Mahanta, S. Shaw, 3D Casson fluid flow past a porous linearly stretching sheet with convective boundary condition, *Alex. Eng. J.*, **54** (2015), 653–659. https://doi.org/10.1016/j.aej.2015.04.014
18. S. Shehzad, T. Hayat, A. Alsaedi, Three-dimensional MHD flow of Casson fluid in porous medium with heat generation, *J. Appl. Fluid Mech.*, **9** (2015), 215–223. https://doi.org/10.18869/ACADPUB.JAFM.68.224.24042
19. C. Raju, N. Sandeep, Unsteady three-dimensional flow of Casson-Carreau fluids past a stretching surface, *Alex. Eng. J.*, **55** (2016), 1115–1126. https://doi.org/10.1016/j.aej.2016.03.023
20. P. Kameswaran, S. Shaw, P. Sibanda, Dual solutions of Casson fluid flow over a stretching or shrinking sheet, *Sadhana*, **39** (2014), 1573–1583. https://doi.org/10.1007/s12046-014-0289-7
21. M. Riaz Khan, M. Elkotb, R. Matoog, N. Alshehri, M. Abdelmohimen, Thermal features and heat transfer enhancement of a casson fluid across a porous stretching/shrinking sheet: analysis of dual solutions, *Case Stud. Therm. Eng.*, **28** (2021), 101594. https://doi.org/10.1016/j.csite.2021.101594
22. M. El-Aziz, A. Afify, MHD Casson fluid flow over a stretching sheet with entropy generation analysis and Hall influence, *Entropy*, **21** (2019), 592. https://doi.org/10.3390/e21060592
23. M. Turkyilmazoglu, Stagnation-point flow and heat transfer over stretchable plates and cylinders with an oncoming flow: exact solutions, *Chem. Eng. Sci.*, **238** (2021), 116596. https://doi.org/10.1016/j.ces.2021.116596
24. L. Ali, B. Ali, M. Ghori, Melting effect on Cattaneo-Christov and thermal radiation features for aligned MHD nanofluid flow comprising microorganisms to leading edge: FEM approach, *Comput. Math. Appl.*, **109** (2022), 260–269. https://doi.org/10.1016/j.camwa.2022.01.009
25. L. Ali, B. Ali, X. Liu, T. Iqbal, R. Zulqarnain, M. Javid, A comparative study of unsteady MHD Falkner-Skan wedge flow for non-Newtonian nanofluids considering thermal radiation and activation energy, *Chinese J. Phys.*, **77** (2022), 1625–1638. https://doi.org/10.1016/j.cjph.2021.10.045

26. P. Kumar, H. Poonia, L. Ali, S. Areekara, The numerical simulation of nanoparticle size and thermal radiation with the magnetic field effect based on tangent hyperbolic nanofluid flow, *Case Stud. Therm. Eng.*, **37** (2022), 102247. https://doi.org/10.1016/j.csite.2022.102247
27. L. Ali, Y. Wu, B. Ali, S. Abdal, S. Hussain, The crucial features of aggregation in TiO_2-water nanofluid aligned of chemically comprising microorganisms: a FEM approach, *Comput. Math. Appl.*, **123** (2022), 241–251. https://doi.org/10.1016/j.camwa.2022.08.028
28. U. Mahabaleshwar, K. Sneha, H. Huang, Newtonian flow over a porous stretching/shrinking sheet with CNTS and heat transfer, *J. Taiwan Inst. Chem. Eng.*, **134** (2022), 104298. https://doi.org/10.1016/j.jtice.2022.104298
29. M. Qureshi, M. Faisal, Q. Raza, B. Ali, T. Botmart, N. Shah, Morphological nanolayer impact on hybrid nanofluids flow due to dispersion of polymer/CNT matrix nanocomposite material, *AIMS Mathematics*, **8** (2023), 633–656. https://doi.org/10.3934/math.2023030
30. A. Rauf, N. Shah, A. Mushtaq, T. Botmart, Heat transport and magnetohydrodynamic hybrid micropolar ferrofluid flow over a non-linearly stretching sheet, *AIMS Mathematics*, **8** (2023), 164–193. https://doi.org/10.3934/math.2023008
31. Y. Lok, N. Amin, I. Pop, Non-orthogonal stagnation point flow towards a stretching sheet, *Int. J. Nonlin. Mech.*, **41** (2006), 622–627. https://doi.org/10.1016/j.ijnonlinmec.2006.03.002
32. C. Wang, Stagnation flow towards a shrinking sheet, *Int. J. Nonlin. Mech.*, **43** (2008), 377–382.
33. J. Shercliff, *A textbook of magnetohydrodynamics*, Oxford: Pergamon, 1965.
34. A. Raptis, C. Perdiki, H. Takhar, Effect of thermal radiation on MHD flow, *Appl. Math. Comput.*, **153** (2004), 645–649. https://doi.org/10.1016/S0096-3003(03)00657-X
35. M. Murad, F. Hamasalh, Computational technique for the modeling on MHD boundary layer flow unsteady stretching sheet by B-spline function, *Proceedings of International Conference on Computer Science and Software Engineering*, 2022, 236–240. https://doi.org/10.1109/CSASE51777.2022.9759738
36. E. Cheney, D. Kincaid, *Numerical mathematics and computing*, New York: Cengage Learning, 2012.
37. P. Prenter, *Splines and variational methods*, New York: Dover Publication, 2008.
38. J. Rashidinia, S. Jamalzadeh, Modified b-spline collocation approach for pricing american style asian options, *Mediterr. J. Math.*, **14** (2017), 111. https://doi.org/10.1007/s00009-017-0913-y
39. V. Mandelzweig, F. Tabakin, Quasilinearization approach to nonlinear problems in physics with application to nonlinear ODEs, *Comput. Phys. Commun.*, **141** (2001), 268–281. https://doi.org/10.1016/S0010-4655(01)00415-5
40. K. Parand, M. Shahini, M. Dehghan, Rational Legendre pseudospectral approach for solving nonlinear differential equations of Lane-Emden type, *J. Comput. Phys.*, **228** (2009), 8830–8840. https://doi.org/10.1016/j.jcp.2009.08.029
41. K. Parand, N. Bajalan, A numerical approach based on B-spline basis functions to solve boundary layer flow model of a non-Newtonian fluid, *J. Braz. Soc. Mech. Sci. Eng.*, **40** (2018), 485. https://doi.org/10.1007/s40430-018-1402-3

AIMS Press